TECHNICAL PAPER

Investigation on controlling the process parameters for improving the quality of investment cast parts

Sarojrani Pattnaik[1]

Abstract

Investment casting is a highly flexible process which was previously perceived as an expensive process. However, when the process is compared to other optional processes which may require machining or welding, this casting can produce metallic components at highly competitive costs. There are many process variables which affect the process such as die temperature, wax temperature, injection pressure, shell firing temperature and time, cooling rate. In this study, important shell parameters such as preheat temperature, firing temperature and firing time, and melt pouring temperature have been chosen as process variables influencing the quality of the hypoeutectic aluminium–silicon alloy investment casting. The optimal input parametric condition for reduction of linear and volumetric shrinkages and increment of tensile strength of Al–Si 7%–Mg investment casting has been identified as shell preheat temperature of 200 °C, firing temperature of 900 °C, firing time of 7 h and pouring temperature of 600 °C. At this optimal setting, it was found that linear and volumetric shrinkages decreased from 0.65 and 1.89% to 0.381 and 1.546%. The tensile strength of the casting increased from 96 to 121 MPa with regard to the nine experimental runs performed. Microstructural observation revealed that higher shell preheat and pouring temperatures led to augmented porosity, increased secondary dendrite arm spacing (35.53 ± 2.4 μm), larger detrimental iron-rich intermetallics (40.49 ± 25.15 μm) followed by reduced tensile properties of the casting (96 MPa).

Keywords Investment casting · Ceramic shell · Aluminium–silicon alloy · Tensile strength

1 Introduction

Foundries try to cast metallic components so as to closely stick to the design specifications with only minor deviations. However, most of the metals and alloys, especially aluminium alloys, are very much prone to shrinkage which affects the casting quality and dimensional stability [1]. The quantitative and qualitative analyses of shrinkage characteristic of the castings help in increasing their mechanical properties. During solidification of melt, its density changes because of cooling of melt in both liquid and solid states in addition to owing to liquid- to solid-phase transformation. In the solid state, phase

transformations also cause a volumetric change which affects the solidification process. The superheated liquid melt cools to the liquidus temperature where solidification begins. During the cooling process, thermal contraction of the melt occurs owing to the lowered temperature. The solidification is also connected to a density change.

The shrinkage could arise at a specific temperature or distributed over a range depending on the solidifying melt. The melt experiences thermal contraction during subsequent cooling, and uneven cooling induces stresses and strains in the cast parts, thereby causing dimensional variations. The shrinkage is influenced by cooling conditions, alloy content and casting temperature [2]. Among various casting processes, investment casting (IC) is a specialized technique which produces components having complicated geometry, necessitates superior surface finish and high-dimensional tolerance [3, 4]. But, IC process involves several nonlinear physical processes which demand for consideration of part geometry, material property, ceramic mould sintering temperature, mould

✉ Sarojrani Pattnaik
  rani_saroj7@yahoo.co.in

1 Department of Mechanical Engineering, Veer Surendra Sai University of Technology, Burla, Odisha, India

preheat temperature, solidification phenomenon of melt, etc. [5]. However, it is seen that the investment cast parts have dimensions slightly smaller than those of the die cavity due to shrinkages of wax pattern and alloy material during solidification.

In the past, many studies have been made regarding reducing wax pattern shrinkages in IC process. Bonilla et al. [6] suggested simulational studies based on computer-aided heat transfer phenomenon to forecast contractions occurring in the wax pattern used in the IC process. Rezavand and Behravesh [7] studied about the dimensional constancy of the wax patterns used to manufacture turbine blades which were produced by wax injection moulding. The process parameters chosen as variables were holding time and injection temperature. It was found that the holding time was significant as regard injection time in reducing pattern shrinkage. Yarlagadda and Hock [8] found the correctness of wax patterns manufactured by hard and soft tooling and further optimized the injection process parameters to achieve good dimensional accurateness of the patterns. Further, Pattnaik et al. [9–11] determined the best wax blend composition made from different types of waxes and fillers and also optimized the injection process parameters so as to reduce pattern shrinkage at the same time improving surface finish and hardness.

IC process utilizes ceramic shell as moulds to cast components, and these shells are built over the wax patterns. The ceramic shells are made from different refractory materials, binders, additives, etc., so as to get enough strength to hold the hot melt. Besides strength, the shell should be adequately permeable and un-reactive in nature. Many studies on ceramic shell building process have been made to investigate the compatibility of chosen moulding material with that of the cast alloy. Since many years, alumina has been employed as the mould primary/face coat material for IC of titanium alloys. Cheng et al. [12] investigated the interface between alumina face coat and titanium aluminide alloy by modelling the cooling profile of the mould during casting. It was found that a high mould preheat temperature and large bar diameter increased the interaction between the shell and the TiAl alloy. Oxygen was found penetrating into the metal in the course of decomposition of the face coat materials and silicon from the backup coat was found to interact with the metal during the casting process. Further, Yuan et al. [13] studied about the influence of different shell preheat temperatures on the moulds with CaO-stabilized zirconia facecoat for casting Ti–46Al–8Nb–1B alloy. The authors suggested that the mould preheat temperatures should be less than 1200 °C for casting titanium aluminide alloys.

Once wax pattern shrinkage has been reduced, next step is to minimize cast metal shrinkage during solidification. Almost, all cast metals shrink on solidification, but shrinkage rate varies from alloy to alloy depending on solidification temperature of metal or alloy, casting design and dimension, moulding condition, pouring temperature, etc. [14]. Currently, aluminium alloys are extensively used in automotive sector due to its low weight, thereby saving fuel consumption [15]. Aluminium–silicon (Al–Si) alloys are significantly used in industries because they display low density, high strength to weight ratio, high wear resistance, low coefficient of thermal expansion. Silicon provides low shrinkage and high fluidity which leads to qualitative casting. However, the cast aluminium alloys are subjected to shrinkage defects [16].

This defect leads to the reduction of mechanical properties such as tensile strength of the casting. Therefore, an analysis has been made by the author to reduce both linear and volumetric casting shrinkage and to increase the tensile strength of the cast part. For this analysis, hypoeutectic Al–Si 7%–Mg alloy for casting in ceramic shells has been used. On the basis of literature survey [17–22], significant process parameters chosen for the study are shell preheat temperature, firing temperature, firing time and pouring temperature to identify their effect on casting shrinkage (both linear and volumetric) and tensile strength of the part produced via IC, while other parameters such as shell thickness, shell drying time, pouring time and cooling condition were kept nearly constant. The range of all the selected input process parameters were decided from the state of the art survey on aluminium alloy castings [23–26] and trial experiments conducted prior to the final experimentation.

Eventually, a set of optimized process parameters have been identified to reduce the shrinkage defects and to enhance the tensile strength of the investment cast part.

2 Materials and methods

First the wax pattern is dipped into ceramic slurry (primary slurry) and drained to get an even wet coating. Then, primary stucco consisting of coarse ceramic grit is applied over the wet coating and dried. The grit adheres to the wet ceramic coating (Fig. 1a). Then, in the similar way, secondary layer is built up over the primary layer. But with a difference that the secondary layer is made from coarser flour and coarser stucco as compared to primary layer (Fig. 1b). Gradually, secondary stucco size is increased to enhance the porosity of the ceramic shell (Fig. 1c). Finally, a seal coat is given to the shell. Total five layers are given to all shells so as to obtain near about uniform shell thickness. After drying, the shell is dewaxed and then fired in an open top muffle furnace at temperatures in the range between 700 and 900 °C.
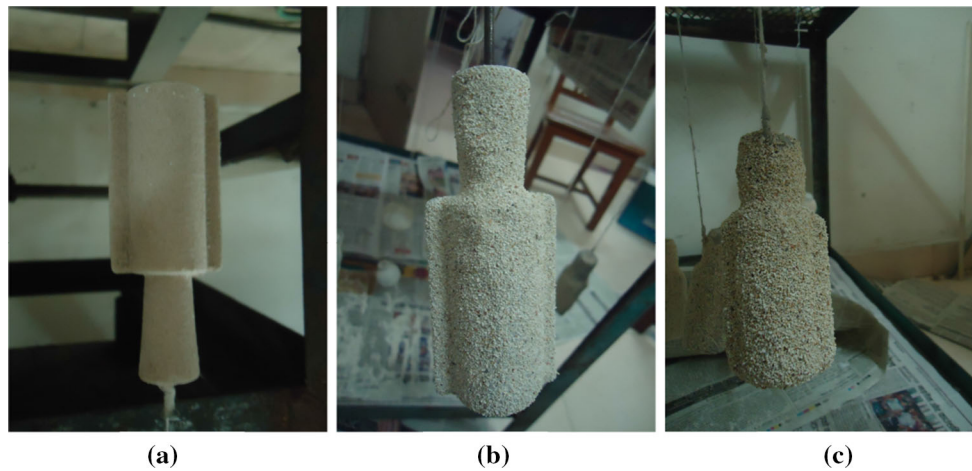
Fig. 1 Ceramic shell building process **a** Facecoat with zircon stucco, **b** first secondary coat with Molochite 30/60 stucco, **c** secondary coats with Molochite 16/30 stucco

The alloy was prepared by liquefying aluminium ingot of 99.9% purity with Al–50% Si master alloy and pure magnesium metal (wrapped in an aluminium foil) in a graphite crucible, using a pit furnace at 800 °C for about 1 h. The molten alloy was treated with flux and degasser to remove impurities and gases. EDX microanalysis of the prepared alloy was done to check the amount of iron content, and subsequently, manganese was added to the mixture at Mn/Fe ratios of ~ 0.5, to reduce the detrimental effects of iron content in the alloy. Then, the melt was poured in the sand mould as shown in Fig. 2a.

The present research work was done solely for academic purpose. The Al–Si alloy for investment casting was prepared using sand mould instead of ingot mould because latter type of mould would require many number of small ingot moulds for preparing about 25 Kgs of aforementioned alloy, which would have been a costly venture. Further, cutting of the cast ingots into small pieces for carrying out each of the experimental runs would increase the lead time of production. It was found that the sand cast

alloy easily broke into small pieces by giving a blow at the gates of the prepared alloy, and accordingly, alloy melting was done to carry out each set of experiments. Finally, the prepared Al–7%Si–Mg alloy was again remelted and poured in ceramic shells as per each of the input parametric condition (Fig. 2b).

3 Experimentation

The process parameters, namely shell preheat temperature, firing temperature, firing time and pouring temperature, were selected to identify their effect on shrinkages occurring in casting and tensile strength of the parts produced via IC. The selected input parameters with their designated symbols and limits are shown in Table 1. The shell preheat temperature was varied in the range between 200 and 400 °C, firing temperature of the ceramic shell in the range between 700 and 900 °C, firing time in the range between 5 and 7 h, and pouring temperature of the melt in the range

Fig. 2 **a** Prepared Al–Si 7%–Mg alloy, **b** investment casting in ceramic shells
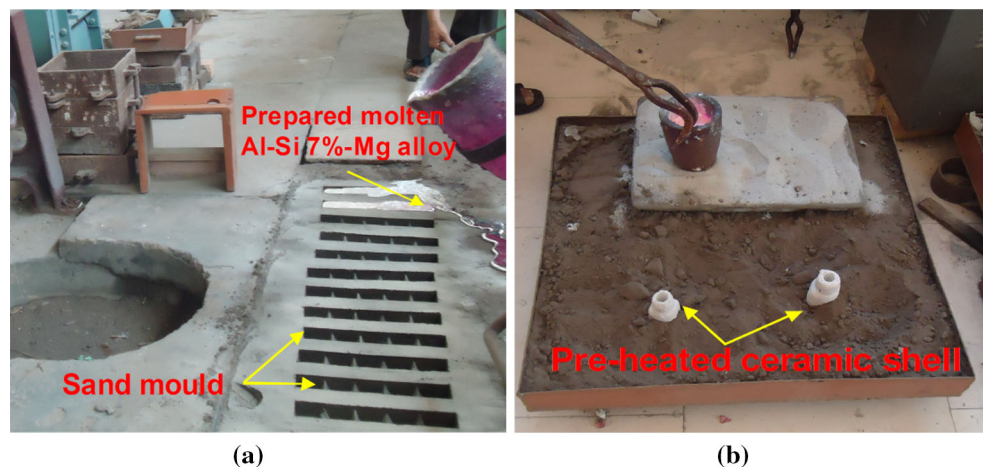
Table 1 Process parameters for IC process

Sl. no.	Input parameter	Symbol	Unit	Level 1	Level 2	Level 3
1	Shell preheat temperature	A	°C	200	300	400
2	Firing temperature	B	°C	700	800	900
3	Firing time	C	h	5	6	7
4	Pouring temperature	D	°C	600	650	700

between 600 and 700 °C, respectively. Taguchi's L9 orthogonal array (OA) was used to conduct the experiments. The allocation of the input process parameters is given in Table 2. The IC parts produced at nine experimental runs were tested for linear shrinkage (LS), volumetric shrinkage (VS) and tensile strength (TS). The ambient temperature during casting was in the range of 25–30 °C.

The linear dimensions of the casting were determined using a digital vernier calliper, and then the LS of the casting was computed using Eq. 1. The casting's volumetric shrinkage was determined by means of Eq. 2. The results obtained by the conduct of experiments for determining the aforementioned responses are also furnished in Table 2. Nine different set of experiments were performed at the trial condition, and for each set of experiments, two replicas have been cast each time. The tensile specimens of the casting were prepared as per ASTM standard E-8/E8 M.

$$LS = \frac{\text{Casting dimension} - \text{Pattern dimension}}{\text{Pattern dimension}} \times 100 \tag{1}$$

$$VS = \frac{\text{Theoretical volume} - \text{Actual volume}}{\text{Theoretical volume}} \times 100 \tag{2}$$

The macrostructural and microstructural investigations were made using optical microscope and scanning electron microscope (SEM), respectively. The secondary dendrite arm spacing (SDAS) values of aluminium grains of the prepared alloy were measured by line intercept (LI) method using Image J software, as shown in Eq. 3. In this method, first several straight line-segments are drawn over the images and the total numbers of grains intersected by each line segments are counted. Then, the length of each line segment is divided by average number of grains intersecting it. This counting process is repeated until 20 different trials are completed. Finally, the average of the number of grains is calculated in microns.

$$\text{Grain size} = \frac{\text{Line length}}{\text{No. of grains}} \tag{3}$$

4 Optimization of responses

Taguchi's analysis of means (ANOM) of the experimental results was computed to determine the optimal parametric condition that will give the best casting characteristics. ANOM for LS, VS and TS of conventional IC is presented in Tables 3, 4 and 5, and the corresponding response graphs are plotted in Fig. 3. It is obvious from the tables that the pouring temperature is the most important

Table 2 Experimental results of various parametric combinations of hypoeutectic IC parts

Sl. no.	Input process parameter				Response								
					LS (%)			VS (%)			TS (MPa)		
	A	B	C	D	R_1	R_2	Mean	R_1	R_2	Mean	R_1	R_2	Mean
1	200	700	5	600	0.44	0.42	0.43	1.58	1.52	1.55	110	116	113
2	200	800	6	650	0.56	0.52	0.54	1.67	1.75	1.71	100	108	104
3	200	900	7	700	0.49	0.47	0.48	1.66	1.62	1.64	106	108	107
4	300	700	6	700	0.64	0.62	0.63	1.79	1.87	1.83	99	95	97
5	300	800	7	600	0.44	0.5	0.47	1.58	1.56	1.57	113	109	111
6	300	900	5	650	0.62	0.54	0.58	1.75	1.77	1.76	102	104	103
7	400	700	7	650	0.57	0.65	0.61	1.76	1.82	1.79	99	99	99
8	400	800	5	700	0.67	0.63	0.65	1.92	1.86	1.89	93	99	96
9	400	900	6	600	0.49	0.55	0.52	1.69	1.67	1.68	107	105	106

A shell preheat temperature (°C), *B* firing temperature (°C), *C* firing time (h), *D* pouring temperature (°C), *LS* linear shrinkage (%), *VS* volumetric shrinkage (%), *TS* tensile strength (MPa)

Table 3 ANOM table for LS of the investment cast part

Symbol	Process parameter	Linear shrinkage (%)			Range	Rank
		Level 1	Level 2	Level 3		
A	Shell preheat temperature	0.4833*	0.5600	0.5933	0.1100	2
B	Firing temperature	0.5567	0.5533	0.5267*	0.0300	4
C	Firing time	0.5533	0.5633	0.5200*	0.0433	3
D	Pouring temperature	0.4733*	0.5767	0.5867	0.1133	1

*Optimal level, total mean of LS = 0.5455

Table 4 ANOM table for VS of the investment cast part

Symbol	Process parameter	Volumetric shrinkage (%)			Range	Rank
		Level 1	Level 2	Level 3		
A	Shell preheat temperature	1.6333*	1.7200	1.7867	0.153	2
B	Firing temperature	1.7233	1.72333	1.6933*	0.030	4
C	Firing time	1.7333	1.7400	1.6667*	0.073	3
D	Pouring temperature	1.6000*	1.7533	1.7867	0.187	1

*Optimal level, total mean of VS = 1.7133

Table 5 ANOM table for TS of the investment cast part

Symbol	Process parameter	Tensile strength (MPa)			Range	Rank
		Level 1	Level 2	Level 3		
A	Shell preheat temperature	108.0*	103.7	100.3	7.7	2
B	Firing temperature	103.0	103.7	105.3*	2.3	4
C	Firing time	104.0	102.3	105.7*	3.3	3
D	Pouring temperature	110.0*	102.0	100.0	10.0	1

*Optimal level, total mean of TS = 104

process parameter influencing all the responses (ranked no. 1 in all cases), which is followed by shell preheat temperature. From the response graph, the optimal parametric condition for all the chosen responses is found to be $A_1B_3C_3D_1$, i.e. shell preheat temperature at 200 °C, firing temperature at 900 °C, firing time of 7 h and pouring temperature of 600 °C. Again, analysis of variance (ANOVA) for LS, VS and TS was computed to verify the outcomes predicted by ANOM. ANOVA tables for LS, VS and TS of conventional IC are reported in Tables 6, 7 and 8. It is apparent from the tables that the percent contribution of pouring temperature is highest for all the responses and all the process parameters are found to be significant.

5 Confirmatory experiments

The optimal value of each response at the predicted optimal condition has been predicted by Taguchi method, and later, confirmatory experiments have been conducted at the same condition. In statistics, the mean absolute percentage error (MAPE) is used to measure the prediction accuracy of a forecasting method and its formula is given by Eq. 4. The summary of Taguchi predicted and the actual experimental results, for all the responses, is presented in Table 9.

$$\text{MAPE} = \left(\frac{1}{n}\sum \frac{|\text{Actual} - \text{Forecast}|}{|\text{Actual}|}\right)*100 \qquad (4)$$

MAPE for all response parameters show less than 10%, which shows a good agreement between the experimental values and numerical values as predicted by Taguchi method. It is clearly seen that the casting shrinkages (both LS and VS) are least and TS is highest at the obtained optimal setting, as compared to the results obtained for each experimental run of L_9 OA. Thus, it shows that the Taguchi predicted optimal condition improved the quality of the IC.

6 Microstructural analysis

The optical micrographs of Al–Si 7%–Mg investment casting at different shell preheat and pouring temperatures are shown in Fig. 4. Figure 4a, b corresponds to the
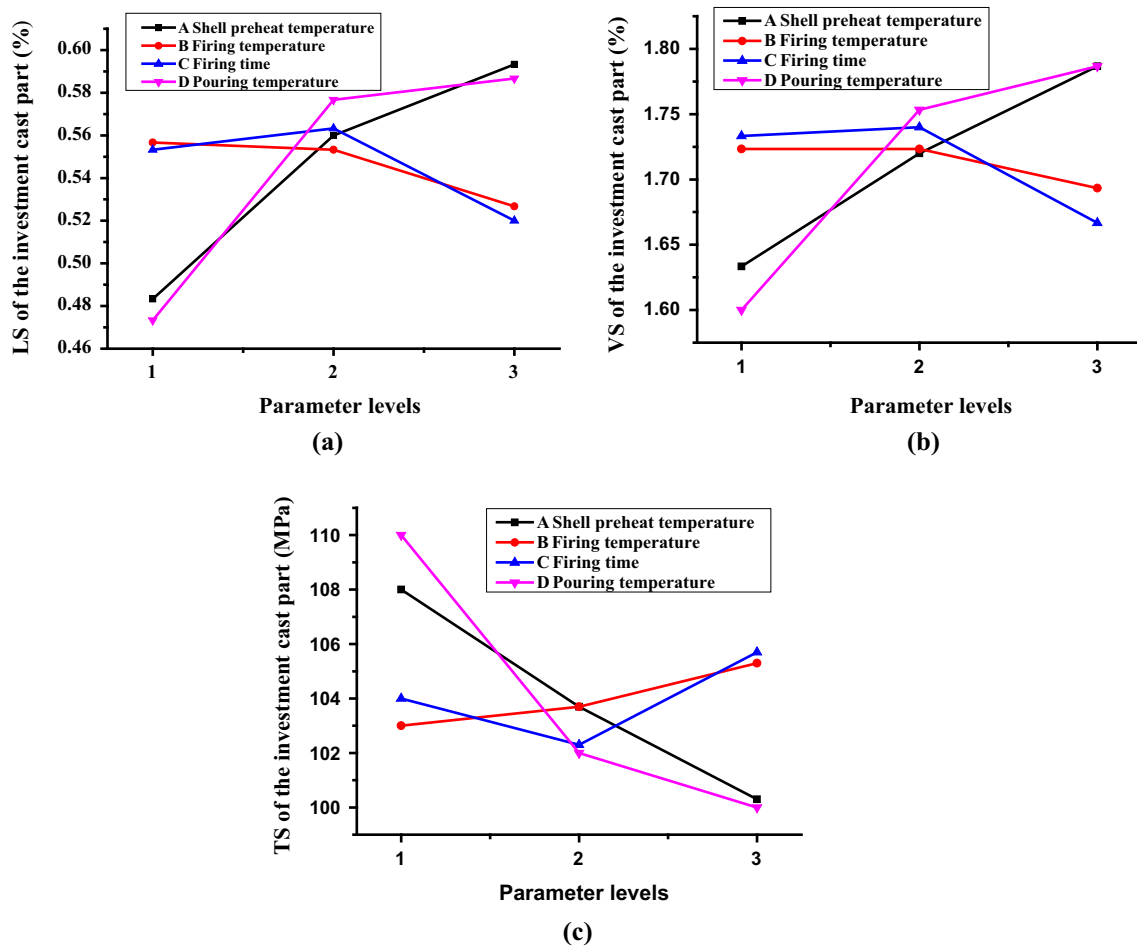
Fig. 3 Response graphs of the IC part showing different responses verses Parameter levels a LS, b VS, c TS

Table 6 ANOVA table—LS of IC

Symbol	Process parameter	Linear shrinkage (%)				
		SS	DOF	V	F-ratio*	P %
A	Shell preheat temperature	0.018873	2	0.009437	1783.9	39.80
B	Firing temperature	0.001838	2	0.000919	173.69	3.87
C	Firing time	0.003086	2	0.001543	291.73	6.51
D	Pouring temperature	0.02353	2	0.011765	2224.0	49.62
E	Error	9.52E − 05	18	5.29E − 06		0.20
T	Total sum	0.047422	26			100

SS sum of squares, DOF degree of freedom, V variance, F-ratio variance ratio, P percentage
*Significant at 95% confidence level

microstructure of the castings produced as per eight and sixth experimental runs of L9 OA (Table 2), whereas Fig. 4(c) corresponds to the confirmatory optimal setting. It can be seen that larger-sized pores are formed at higher shell preheat and pouring temperatures (Fig. 4a). However, the pore size decreases with a decrease in aforementioned temperatures.

SDAS of aluminium grains of Al–Si 7%–Mg investment cast part at different shell preheat and pouring temperatures has been computed and is shown in Table 10. It is obvious from the table that the SDAS is larger when the aforementioned temperatures are higher, whereas SDAS is reduced when the shell preheat and pouring temperatures are less.

Table 7 ANOVA table—VS of IC

Symbol	Process parameter	Volumetric shrinkage (%)				
		SS	DOF	V	F-ratio*	P %
A	Shell preheat temperature	0.032204	2	0.016102	1053.0	30.21
B	Firing temperature	0.001697	2	0.000849	55.499	1.59
C	Firing time	0.009734	2	0.004867	318.30	9.13
D	Pouring temperature	0.06269	2	0.031345	2049.9	58.81
E	Error	0.000275	18	1.53E−05		0.26
T	Total sum	0.1066	26			100

Table 8 ANOVA table—TS of IC

Symbol	Process parameter	Tensile strength (Mpa)				
		SS	DOF	V	F-ratio*	P %
A	Shell preheat temperature	68.811	2	34.405	566.79	24.40
B	Firing temperature	8.340	2	4.17	68.696	2.96
C	Firing time	35.757	2	17.878	294.52	12.68
D	Pouring temperature	168.000	2	84.00	1383.8	59.57
E	Error	1.093	18	0.061		0.89
T	Total sum	282.000	26			100

Table 9 Optimal process condition for responses LS, VS and TS in case of IC

Response	Unit	Optimal settings	Taguchi predicted result	Experimental result	MAPE (%)
LS	%	$A_1B_3C_3D_1$	0.367	0.381	3.67
VS	%	$A_1B_3C_3D_1$	1.453	1.546	6.02
TS	MPa	$A_1B_3C_3D_1$	117.0	121.0	3.31
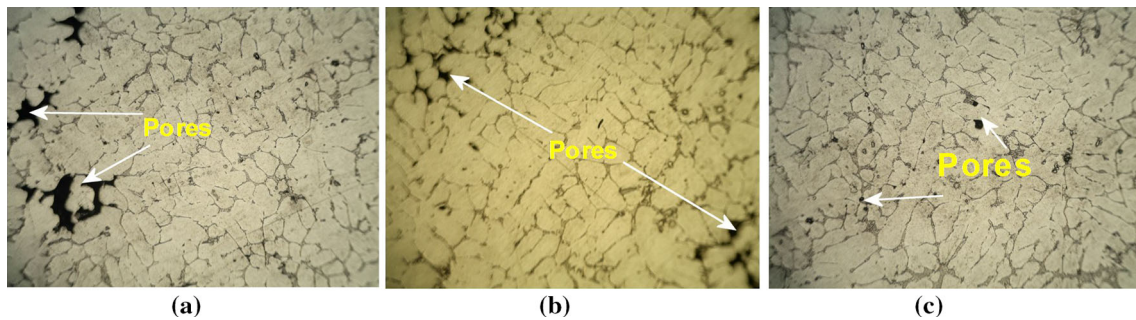
Fig. 4 Optical micrograph (100X) of investment cast Al–Si 7%–Mg part at respective shell preheat and pouring temperatures of **a** 400 and 700 °C, **b** 300 and 650 °C, **c** 200 and 600 °C

Table 10 Average SDAS of Al–Si 7%–Mg investment cast part at different shell preheat and pouring temperatures
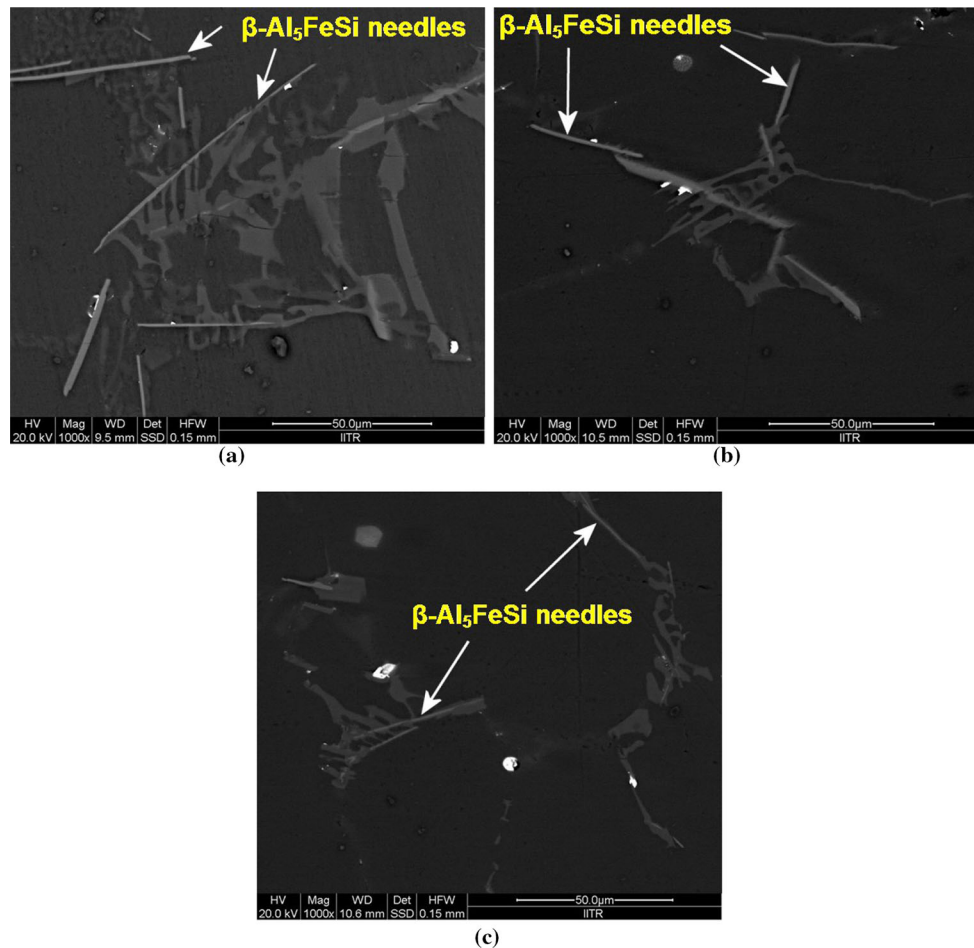
Sl. no.	Shell preheat temperature (°C)	Pouring temperature (°C)	SDAS (μm)	
			Average	SD
1	400	700	35.53	2.40
2	300	650	32.69	1.04
3	200	600	29.49	4.84

Further, the most unfavourable iron-rich intermetallic compounds found in aluminium alloys known as β-Al₅FeSi needles which reduce the mechanical properties of the casting were found in all the three cases and are tabulated in Table 11 and shown in Fig. 5. It is found that with an increase in shell preheat and pouring temperatures, the

Table 11 Average length of β-Al$_5$FeSi needles of Al–Si 7%–Mg investment cast part at different shell preheat and pouring temperatures

Sl. no.	Shell preheat temperature (°C)	Pouring temperature (°C)	β-Al$_5$FeSi needles (μm)	
			Average	SD
1	400	700	40.49	25.15
2	300	650	32.59	13.96
3	200	600	27.64	11.64

Fig. 5 SEM micrographs of the β-Al$_5$FeSi needles of Al–Si 7%–Mg investment cast part at different shell preheat and pouring temperatures **a** 400 and 700 °C, **b** 300 and 650 °C, **c** 200 and 600 °C

number as well as the length of β-Al$_5$FeSi needles increases, whereas the size and quantity of these needles decrease with a decrease in aforesaid temperatures which is beneficial for the casting.

The tensile strengths of the Al–Si 7%–Mg investment cast part at different shell preheat and pouring temperatures are summarized in Table 12. It is found that the tensile strength and ductility of the casting increase with a decrease in aforementioned temperatures. Further, fractography of the tensile specimen at these three different casting conditions were performed as shown in Fig. 6. It is clearly seen that Fig. 6(a) exhibits a river pattern of brittle fracture, whereas Fig. 6b, c displays dimple morphology.

When the shell preheat and pouring temperatures are least, i.e. case-III, more no. of large-sized dimples are seen.

7 Discussions

Ceramic shells are fired (a) to remove residual pattern material and solvents remaining in the ceramic after dewaxing, (b) to sinter the structure of the ceramic, (c) to present the mould for casting at a predetermined and consistent temperature. High shell firing temperature ensures rapid removal of residue and high mould stability. If shell firing temperature and firing time are not proper,

Table 12 Average tensile strengths of Al–Si 7%–Mg investment cast part at different shell preheat and pouring temperatures

Sl. no.	Shell preheat temperature (°C)	Pouring temperature (°C)	Tensile strength (MPa)	Elongation (%)
1	400	700	96	2.1
2	300	650	103	2.3
3	200	600	121	3.3

Fig. 6 SEM fractographs of Al–Si 7%–Mg investment cast tensile samples obtained at different shell preheat and pouring temperatures **a** 400 and 700 °C, **b** 300 and 650 °C, **c** 200 and 600 °C

(a)

(b)

(c)
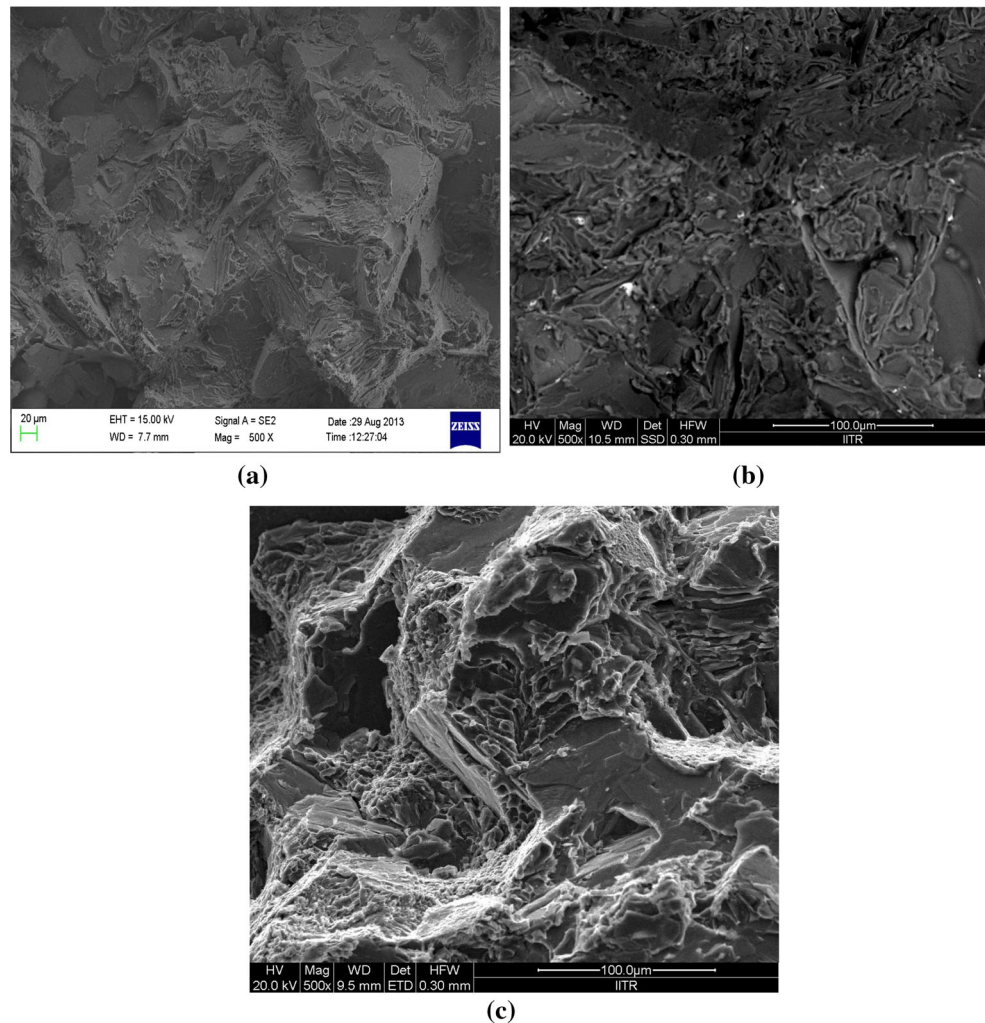
absorbed traces of waxes, dirt or impurities present in the ceramic shell reacts with the hot melt on the surface of the melt. Further, the water or moisture present in the mould would be unable to move out of the shell and produce open blows and blow holes in the casting while coming in contact with the melt, thereby reducing the mechanical properties of the casting. It is seen from the present study that the optimal firing temperature and firing time are at (highest) level 3, i.e. 900 °C and 7 h. Thus, high firing temperature and time played a role in increasing the tensile strength of the investment casting. Additionally, when a ceramic shell is properly fired, the pores present in it get open and thus, casting solidifies very quickly which diminishes the occurrence of casting shrinkage.

When the shell preheat temperature is less, cooling rate is fast, which leads to finer microstructure, and it also results in narrow solidification bands, which improves the feeding inside the casting, thereby increasing the mechanical properties as well as reducing the shrinkages occurring in the cast parts. When the shell preheat temperature increases, gases like hydrogen are easily formed in the molten alloy and cause defects, such as, gas and

shrinkage porosities, and solidification shrinkage, which hampers the mechanical property, such as tensile strength of the cast parts. This is due to the development of high thermal gradients, which slows the rate of cooling, and hence there is a reduction of radiative heat transfer coefficient, which consecutively decreases the tensile strength, thus obtained.

Though high pouring temperature increases the supply of molten metal at the interdendritic cavities, simultaneously, it amplifies the dissolution of hydrogen inside the molten metal. During cooling of the casting, the liquefied hydrogen leaks out of the melt, owing to its inferior dissolvability at reduced temperatures, whereas a little quantity of the emerged gas is captured in the freezing casting, thereby increasing the porosity in it. Further, the higher the degree of superheat exists in the melt, the higher is the solidification time of the casting. Therefore, tensile strength is reduced with an increase in pouring temperature. Higher pouring temperature of the molten alloy in the ceramic shells cause slower solidification, which in turn leads to the formation and growth of iron-rich intermetallics (the β-Al$_5$FeSi needles) usually found in aluminium alloys. These intermetallics are very much detrimental to the mechanical properties of the cast parts, due to its brittle nature. It causes severe feeding difficulties during solidification and ultimately, leads to shrinkage porosity formation, due to the precipitation of coarse β-Al$_5$FeSi needles, which blocks the interdendritic flow channels. Higher cooling rates could refine the β-Al$_5$FeSi needles formed inside the castings. Thus, the lesser the shell preheat temperature and alloy pouring temperature, the higher the mechanical properties and lesser is the shrinkage problem in the casting.

The mechanical properties of the castings are influenced by SDAS [27], and Lim et al. [28] found that a reduction in SDAS value augments the tensile strength and elongation values of the cast parts. SDAS is directly proportional to the local solidification time as given by Eq. 5.

$$SDAS \propto t_s^{-n} \tag{5}$$

where 't_s' is the local solidification time in s and 'n' is an exponent whose value usually lies between 0.3 and 0.4. It can be seen from Table 11 that the average SDAS of Al–Si 7%–Mg investment cast part is minimum when the shell preheat and pouring temperatures are minimum, which clearly shows that due to less local solidification times, average SDAS was least for the aforesaid case.

8 Conclusions

From the above research work, the following conclusions are drawn:

- The optimal input parametric condition for reduction of linear and volumetric shrinkages and increment of tensile strength of Al–Si 7%–Mg investment casting is found to be $A_1B_3C_3D_1$, i.e. shell preheat temperature of 200 °C, firing temperature of 900 °C, firing time of 7 h and pouring temperature of 600 °C. At this optimal setting, LS, VS and TS are found to be 0.381, 1.546% and 121 MPa, respectively, and these values are the best among the nine experimental runs performed.
- Larger-sized pores inside the casting are formed at higher shell preheat temperature, i.e. 400 °C and higher pouring temperature, i.e. 700 °C.
- With the increase in shell preheat temperature and pouring temperature from 200 and 600 °C to 400 and 700 °C, the SDAS size increased from 29.49 ± 4.84 to 35.53 ± 2.4 µm and the length of β-Al$_5$FeSi needles increased from 27.64 ± 11.64 to 40.49 ± 25.15 µm, which is very much detrimental.
- The tensile strength and elongation of the casting increased from 96 MPa and 2.1% to 121 MPa and 3.3% by decreasing the melt pouring temperature and shell preheat temperature to 200 and 600 °C. Further, fractography of the tensile specimen showed that a decrease in aforementioned temperatures led to dimpled morphology, thereby reducing the brittleness of the material.

References

1. Casting (1998) ASM international, ASM metals handbook, vol 15. The Materials Information Company
2. Calcom SA (2001) Simulating porosity in ductile iron castings. Parc Scientifique EPFL, CH-1015 Lausanne, Switzerland
3. Pattnaik SR, Karunakar DB, Jha PK (2012) Developments in investment casting process—a review. J Mater Process Technol 212:2332–2348
4. Pattnaik SR, Karunakar DB, Jha PK (2013) Multi-characteristic optimization of wax patterns in the investment casting process using grey–fuzzy logic. Int J Adv Manuf Technol 67:1577–1587
5. Dong YW, Li XL, Zhao Q, Yang J, Dao M (2017) Modeling of shrinkage during investment casting of thin-walled hollow turbine blades. J Mater Process Technol 244:190–203
6. Bonilla W, Masood SH, Iovenitti P (2001) An investigation of wax patterns for accuracy improvement in investment cast parts. Int J Adv Manuf Technol 18:348–356
7. Rezavand SAM, Behravesh AH (2007) An experimental investigation on dimensional stability of injected wax patterns of gas turbine blades. J Mater Process Technol 182:580–587
8. Yarlagadda PKDV, Hock TS (2003) Statistical analysis on accuracy of wax patterns used in investment casting process. J Mater Process Technol 138:75–81
9. Pattnaik SR, Karunakar DB, Jha PK (2013) Influence of injection process parameters on dimensional stability of wax patterns made by the lost wax. Proc Inst Mech Eng L J Mater Des Appl 227(1):52–60

10. Pattnaik SR, Karunakar DB, Jha PK (2013) Parametric optimization of the investment casting process using utility concept and Taguchi method. Proc Inst Mech Eng L J Mater Des Appl. https://doi.org/10.1177/1464420713487654

11. Pattnaik SR, Karunakar DB, Jha PK (2013) Modeling and parametric optimization of investment casting process by uniting desirability function approach and fuzzy logic. J Intell Fuzzy Syst. https://doi.org/10.3233/IFS-130809

12. Cheng X, Yuan C, Shevchenko D, Withey P (2014) The influence of mould pre-heat temperature and casting size on the interaction between a Ti–46Al–8Nb–1B alloy and the mould comprising an Al_2O_3 face coat. Mater Chem Phys 146:295–302

13. Yuan C, Cheng X, Holt GS, Shevchenko D, Withey P (2014) Investment casting of Ti–46Al–8Nb–1B alloy using moulds with CaO-stabilized zirconia facecoat at various mould pre-heat temperatures. Ceram Int. https://doi.org/10.1016/j.ceramint.2014.11.109

14. Casting Design and Performance (2009) ASM international. The Materials Information Society, Page, p 62

15. Das S, Mondal DP, Sawla S, Ramkrishnan N (2008) Synergic effect of reinforcement and heat treatment on the two body abrasive wear of an Al–Si alloy under varying loads and abrasive sizes. Wear 264:47–59

16. Flemings MC (1974) Solidification processing. McGraw-Hill Inc., London

17. Arulraj M, Palani PK (2018) Parametric optimization for improving impact strength of squeeze cast of hybrid metal matrix (LM24–SiCp–coconut shell ash) composite. J Braz Soc Mech Sci Eng. https://doi.org/10.1007/s40430-017-0925-3

18. Mishra S, Ranjana R (2010) Reverse solidification path methodology for dewaxing ceramic shells in investment casting process. Mater Manuf Process 25:1385–1388

19. Tian GL, Bu K, Zhao DQ, Zhang YL, Qiu F, Zhang XD, Ren SJ (2018) A shrinkage prediction method of investment casting based on geometric parameters. Int J Adv Manuf Technol 96:1035–1044. https://doi.org/10.1007/s00170-018-1618-5

20. Venkat Y, Singh S, Das DK, Pandey AK (2018) Effect of fine alumina in improving refractoriness of ceramic shell moulds used for aeronautical grade Ni-base superalloy castings. Ceram Int. https://doi.org/10.1016/j.ceramint.2018.03.197

21. Brown RA, Brown CA (1970). Investment shell molds for the high integrity precision casting of reactive and refractory metals, and methods. Patented No. 3,537,949

22. Li YM, Li RD (2001) Effect of casting process variables on microporosity and mechanical properties in an investment cast aluminium alloy. Sci Technol Adv Mater 2:277–280

23. Sidhu BS, Kumar P, Mishra BK (2008) Effect of slurry composition on plate weight in ceramic shell investment casting. JMEPEG 17:489–498. https://doi.org/10.1007/s11665-007-9162-8

24. Beeley PR, Smart RF (1995) Investment casting, 1st edn. The Institute of Materials, London

25. Birol Y (2009) Semi-solid processing of the primary aluminium die casting alloy A365. J Alloys Compd 473:133–138

26. Yang LJ (2003) The effect of casting temperature on the properties of squeeze cast aluminium and zinc alloys. J Mater Process Technol 140:391–396

27. Campbell J (1991) Castings. Butterworths-Heinemann, Oxford, pp 261–268

28. Lim CS, Clegg AJ, Loh NL (1997) The reduction of dendrite ARM spacing using a novel pressure-assisted investment casting approach. J Mater Process Technol 70:99–102